



PII S0016-7037(99)00182-9

## Uptake and fractionation of rare earth elements on hydrothermal plume particles at 9°45'N, East Pacific Rise

ROBERT M. SHERRELL,\*<sup>1</sup> M. PAUL FIELD,<sup>1</sup> and GREG RAVIZZA<sup>2</sup><sup>1</sup>Institute of Marine and Coastal Sciences, Rutgers University, 71 Dudley Road, New Brunswick, NJ 08901-8521, USA<sup>2</sup>Department of Marine Geology and Geophysics, Woods Hole Oceanographic Institution, Woods Hole, MA 02543-1541, USA

(Received December 15, 1998; accepted in revised form May 12, 1999)

**Abstract**—Particulate samples ( $>0.45 \mu\text{m}$ ) from a neutrally buoyant hydrothermal plume at 9°45'N on the northern East Pacific Rise were collected using large volume in situ filtration and analyzed for Fe, Al, Mn, Ni, and fourteen rare earth elements (REE). The Sm/Fe ratio (a proxy for overall REE/Fe) and Nd/Er (light/heavy REE fractionation) increased moderately with decreasing particulate Fe. Chemically, the sense of these relationships matched that documented previously in the TAG plume on the Mid-Atlantic Ridge (German et al., 1990), although particulate Fe was about 10 fold lower at 9°45'N. Spatial trends relative to the vent source, however, were opposite of expectation because slow Fe(II) oxidation and Fe(III) colloid aggregation over this interval led to increased particulate Fe (10–26 nM) with distance from source (Field and Sherrell, submitted). After subtraction of non-plume background particle composition, plume particles at 9°45'N and TAG had indistinguishable ranges of light REE-enriched fractionation relative to ambient seawater and had very similar Sm/Fe (therefore Kd for Fe oxyhydroxides), demonstrating that plume particles in both oceans reflect to a first degree the local seawater REE composition. Within-plume REE variations at 9°45'N were investigated using a simple mixing model which accounts for the bulk Fe-Al-Mn variations in the plume using two endmembers: fresh hydrothermal oxyhydroxide precipitates and ridge-crest background particles (composed largely of locally resuspended sediment). Sm/Fe and Nd/Er plot linearly with mixing ratio ( $R > 0.96$ ), implying that the observed REE trends result from mixing of these two endmembers. Extrapolation to the composition of pure hydrothermal precipitates suggests that Nd/Er is fractionated relative to seawater by a factor of 1.8 during adsorption onto fresh Fe oxyhydroxide particles. The ridge-crest background particles are 5 fold higher in Sm/Fe and Nd/Er is 2.49 relative to seawater, partly a result of enriched terrigenous component in the resuspended matter. A reinterpretation of REE at TAG reveals that positive curvature in REE vs. Fe plots, argued previously to reflect continuous REE uptake (i.e., increasing Kd; German et al., 1990), may result from local depletion of the dissolved REE pool by partitioning onto Fe particles at  $\text{Fe} > 100 \text{ nM}$ . Similar drawdown effects could contribute to the variable degrees of curvature observed for all seawater-source particle-reactive species in plumes that are sampled at high particulate Fe concentration. In sum, REE behavior in hydrothermal plumes is more consistent with equilibrium adsorption and mixing of distinct particle types, than with kinetic uptake control. Precise measurements of REEs in modern ridge-crest metalliferous sediments could be compared to the endmember composition calculated from the plume data to evaluate long-term changes in REE of the hydrothermal component. Copyright © 1999 Elsevier Science Ltd

### 1. INTRODUCTION

Circulation of seawater through the young oceanic lithosphere along mid-ocean ridges results in hydrothermal venting, one of the major inputs of heat and chemicals to the ocean (Humphris et al., 1995). Since the discovery of deep-sea venting the late 1970s, geochemical studies using submersibles have demonstrated that high temperature vent fluids are enriched in some elements by six to nine orders of magnitude relative to ambient seawater (e.g., Fe), and by smaller factors for many other elements, while a few are nearly completely depleted (e.g., Mg) (Michard, 1989; Von Damm, 1995; Von Damm et al., 1995). A number of studies of the chemical dynamics of buoyant and neutrally buoyant plumes in the Atlantic and Pacific have shown that reactions within vent plumes modify the net effects of hydrothermal venting on oceanic elemental budgets (Feely et al., 1999; Feely et al., 1990; Feely et al., 1994a; Feely et al., 1994b; German et al., 1997; German et al., 1991a; Kadko et al.,

1994a; Kadko et al., 1994b; Lupton et al., 1993; Massoth et al., 1994; Metz and Trefry, 1993; Mottl and McConachy, 1990; Mottl et al., 1995; Trocine and Trefry, 1988). These studies have revealed a generally consistent sequence of chemical reactions occurring within plumes. Initially, in the buoyant plume, about half the iron precipitates as sulfides within the first few meters above the vent orifice (Feely et al., 1990; Mottl and McConachy, 1990; Rudnicki and Elderfield, 1993). Rapid dilution and cooling, accompanied by increases in pH and oxygen concentration, lead to precipitation of the remaining Fe as oxides and oxyhydroxides (Massoth et al., 1999; Mottl and McConachy, 1990). In contrast, Mn is very slow to oxidize, even with bacterial catalysis (Cowen et al., 1990), hence Mn oxide particles are only produced over longer time periods in the very distal plume or within ridge-crest surface sediments.

Particle-reactive elements, which are only moderately enriched in vent fluid (relative to seawater), may be rapidly and completely removed by adsorption or coprecipitation with hydrothermal precipitates; continued reaction then draws from the ambient seawater reservoir (Feely et al., 1996; German et al., 1991a; German et al., 1990; Kadko et al., 1994a; Klinkhammer

\*Author to whom correspondence should be addressed (sherrell@imcs.rutgers.edu).

et al., 1983; Trocine and Trefry, 1988). For these elements, deep sea hydrothermal systems act as a net removal flux and generate precipitates within the advecting plume with concentrations of these elements reflecting that of ambient seawater, with negligible chemical signature of the original vent fluid. This paper explores the extent to which this is true for the rare earth elements (REE). We focus on the roles of Fe(II) oxidation kinetics and mixing of primary hydrothermal particles with local background particles in determining REE variations within a neutrally buoyant plume at 9°45'N on the northern East Pacific Rise (NEPR; Haymon et al., 1993).

Seawater-source elements including the REEs (and Be, Y, Th and Pb-210; German et al., 1990) are presently understood to accumulate on plume particles by continuous adsorption as the neutrally buoyant plume is dispersed on time scales of days, leading to increased metal/Fe ratio and positive curvature in the particulate metal vs. Fe regression (German et al., 1997; German et al., 1991a; German et al., 1990). Others have suggested that this process continues on longer time scales as hydrothermal metalliferous sediments accumulate on ridge flanks (Olivarez and Owen, 1989; Ruhlin and Owen, 1986). Evidence for adsorptive scavenging of seawater REEs onto Fe oxyhydroxides in hydrothermal plumes includes depletion of dissolved REEs from plume height in the water column west of the southern East Pacific Rise (SEPR; Klinkhammer et al., 1983), seawater-like REE patterns in plume particles at the TAG site on the Mid-Atlantic Ridge (German et al., 1990), and REE accumulation rates in metalliferous sediments which exceed those of deep sea red clays (Barrett and Jarvis, 1988; Ruhlin and Owen, 1986). Because REEs have only been examined in one hydrothermal plume (TAG: German et al., 1990), it has been difficult to argue the generality of this phenomenon, and to evaluate the relationship between the hypothesized continuous uptake of REEs and the chemical gradients that result from mixing of primary hydrothermal particles with background suspended particles as the plume is diluted.

In the present study, we examine in detail the chemical composition of particles in and near a neutrally buoyant plume on the EPR. We interpret trends in REE composition within the context of processes which drive systematic variations in the bulk Fe-Al-Mn composition of plume particles within a few km of the vent source. Because this is the first investigation of particulate REE behavior in a Pacific plume, we use these data in combination with previously published REE data at the TAG site in the North Atlantic (German et al., 1990) to address the following questions:

1. Does the uptake and inter-element fractionation of REEs in Pacific and Atlantic plumes reflect the composition of ambient deepwater with quantitative consistency?
2. What are the roles of Fe(II) oxidation, Fe(III) colloid aggregation, and mixing with local background particles (including a resuspended component), in driving within-plume trends in particulate REE composition?
3. What are the relative roles of Fe and Mn oxides in governing REE adsorption onto hydrothermal precipitates?
4. Do the data support a process of continued adsorption of REEs on the time scale of near-field plume advection?

## 2. SAMPLING AND ANALYTICAL METHODS

### 2.1. Large Volume In Situ Filtration of Plume Particles

Suspended particulate matter was sampled at the 9°45'N hydrothermal vent region on the EPR (Fig. 1) using large volume in situ filtration from the R/V Atlantis, Voyage 132, Leg 25 from April 6 to 24, 1996. Each hydrowire cast consisted of a CTD, transmissometer, pinger, and two in situ pumps. Because of unreliable performance of an acoustic transponder intended to establish pump coordinates within the ALVIN transponder grid, sample location with respect to hydrothermal vent sites was dependent on ship navigation and the magnitude of transmissometer anomalies within the plumes. Sample locations are shown as a series of coordinate fixes corresponding to estimated drift during the pumping interval (Fig. 1).

Samples were collected from depths of 2340 m to 2440 m (~70 m above bottom). Spacing between pumps on the hydrowire varied from 14 to 21 m; the letters T and B hereafter designate the top and bottom pumps, respectively. Particulate matter was collected on Millipore HA filters (0.45  $\mu\text{m}$  pore size, 142 mm diameter) mounted on the Rotating Automatic Pump for Particulate Inorganics Determination (RAPPID; Sherrell, 1991; Sherrell et al., 1998). Volumes filtered ranged from 700 to 1530 liters, depending on pumping efficiency, battery charge and filter clogging. Upon pump recovery, residual seawater retained in the filter holder headspace was pulled through the filter using a gentle vacuum, and the filter was visually inspected for sample homogeneity. All sampled filters appeared homogeneous with respect to particle distribution and were folded in half and stored frozen prior to subsampling and digestion. Previous experience indicates that visually homogeneous pump filters have a subsampling reproducibility which is always better than  $\pm 10\%$  and often better than  $\pm 3\%$  (Sherrell et al., 1998, unpublished data).

In order to set the plume chemistry results within a spatial context with respect to local vent sources, it is useful to summarize the location of each 2-pump cast in this study. The overall sampling strategy was to collect evolving near-field (<2 km from vent site) neutrally buoyant plume samples associated with known vents. Casts 5, 7 and 10 represent near-source neutrally buoyant plume particles (<300 m from vents L; vent A has no active plume). Casts 6 and 11 were located further to the west-northwest, and are assumed to represent material which has been transported further from vent L in the prevailing westerly currents (Fig. 1). Age of plume water sampled is difficult to estimate; regional geostrophic calculations give a mean near-bottom current of 5  $\text{cm sec}^{-1}$  (Reid, 1982), corresponding to a plume advection rate of ~4.3 km/day, and an age for Cast 11 plume water of about 8 hours. However, the possible importance of variable tidal currents is poorly known; instantaneous current speeds could vary at least a factor of three on either side of this estimate.

Other casts represent samples collected outside of the main axis of mean plume advection defined by Casts 7, 10, 6 and 11 (Fig. 1). Cast 4 was deployed just west of the ridge axis, ~1 km north of L vent, in the vicinity of V vent, thus far a poorly characterized black smoker (sampled 12/97, 342°C). Cast 2 was taken while towing parallel to the axis from a point roughly midway between P and L vents (Fig. 1). This tow occurred

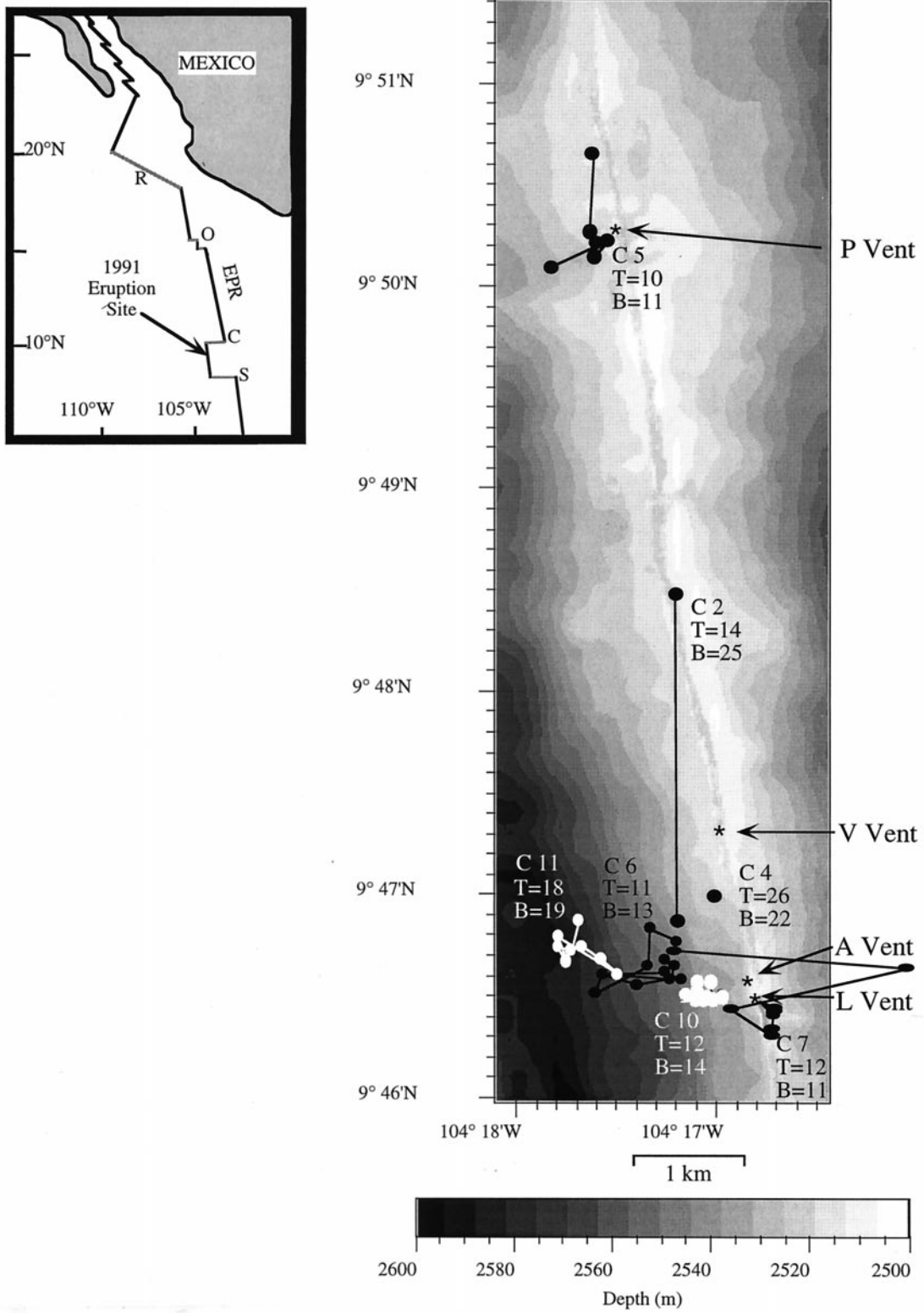


Fig. 1. Location map of neutrally buoyant plume samples collected from 9°46–51'N vent sites along the East Pacific Rise. Known high-temperature vents are shown as stars. Station cast locations are indicated as a series of coordinate fixes during the 3–4 hr filtration (Cast 2 is a towed transect). Values marked T and B indicate particulate Fe concentrations (nM) for top and bottom pumps samples in each cast. A “background” sample (Cast 3) was collected ~10 km east of the ridge at 2100 m depth (not shown).

Table 1. Particulate concentrations of trace metals at 9°45'N on the East Pacific Rise (Fe, Al, Mn in nM, all others in pM).

Cast #	Fe	Al	Mn	Ni	La	Ce	Pr	Nd	Sm	Eu	Gd	Tb	Dy	Ho	Er	Tm	Yb	Lu
3B*	1.0	3.45	0.08	21.8	0.36	0.87	0.073	0.29	0.060	0.0148	0.060	0.0089	0.057	0.0128	0.040	0.0058	0.041	0.0062
2B	24.8	4.15	1.48	14.5	1.76	1.43	0.426	1.80	0.394	0.1057	0.439	0.0667	0.429	0.0911	0.268	0.0382	0.239	0.0344
2T	14.0	4.27	1.18	16.8	1.18	1.17	0.274	1.15	0.247	0.0659	0.270	0.0417	0.265	0.0565	0.164	0.0239	0.148	0.0216
4B	22.2	3.44	1.14	12.8	1.29	0.94	0.307	1.31	0.286	0.0777	0.321	0.0502	0.321	0.0688	0.200	0.0289	0.178	0.0259
4T	25.6	3.97	1.40	17.3	1.60	1.21	0.388	1.64	0.360	0.0984	0.405	0.0632	0.399	0.0859	0.249	0.0366	0.224	0.0332
5B	11.3	4.30	1.48	17.5	1.16	1.18	0.277	1.17	0.246	0.0643	0.264	0.0403	0.255	0.0539	0.157	0.0224	0.140	0.0206
5T	10.3	3.91	1.34	15.8	1.17	1.18	0.276	1.15	0.245	0.0644	0.263	0.0400	0.254	0.0537	0.156	0.0223	0.140	0.0202
6B	13.2	4.60	1.66	18.5	1.45	1.43	0.342	1.43	0.302	0.0799	0.323	0.0499	0.314	0.0664	0.193	0.0278	0.172	0.0253
6T	10.8	3.85	1.31	12.5	1.14	1.17	0.271	1.13	0.240	0.0635	0.259	0.0396	0.251	0.0530	0.154	0.0224	0.138	0.0203
7B	10.8	3.70	1.44	16.2	1.20	1.17	0.282	1.18	0.251	0.0661	0.269	0.0416	0.261	0.0554	0.160	0.0229	0.145	0.0215
7T	12.2	4.01	1.40	13.9	1.20	1.24	0.286	1.20	0.254	0.0678	0.272	0.0426	0.266	0.0567	0.164	0.0239	0.148	0.0217
10B	13.6	3.57	1.22	12.1	1.12	1.07	0.263	1.10	0.236	0.0626	0.256	0.0390	0.247	0.0522	0.152	0.0220	0.136	0.0199
10T	11.5	3.16	1.23	13.4	1.12	1.15	0.267	1.12	0.238	0.0629	0.255	0.0393	0.246	0.0525	0.153	0.0223	0.136	0.0199
11B	19.0	4.64	1.58	17.0	1.47	1.31	0.353	1.49	0.318	0.0850	0.345	0.0537	0.337	0.0717	0.210	0.0304	0.187	0.0275
11T	18.0	4.10	1.43	14.0	1.35	1.25	0.327	1.37	0.294	0.0783	0.321	0.0496	0.312	0.0667	0.193	0.0279	0.173	0.0252

\* Off-axis background sample.

because no transmissometry anomaly was detected, and ship operations required repositioning. To allow a comparison of near-source neutrally buoyant plume material from two distinct high temperature vent systems, Cast 5 was deployed just west of P vent (Fig. 1). Cast 3, located ~10 kilometers east of the ridge axis (9°46'N, 104°22'W) at 2100 m depth, was assumed to sample background particulate material at depths similar to that of the neutrally buoyant plume. During Cast 3, pump T remained off so that its filter could be used as a “dipped” process blank.

To ensure that the pumps remained within the plume during the ~4-hour sampling period, pump B (located 7 m above the transmissometer) was navigated to maintain a continuous position at the base of the maximum transmissometry anomaly; we estimate it sampled plume water >90% of the time. Pump T samples can be considered near-replicates of pump B samples, with differences in sample composition reflecting <21m-scale vertical inhomogeneities within the plume. Transmissometry profiles often showed double or fingered peaks; maximum anomalies varied from 0.35% for Cast 10 to 0.15% for Cast 6, to a broad and barely resolvable ~0.02% for Cast 4. Both Casts 2 and 4 were collected “blindly” since no %T anomalies were evident during real-time monitoring of the CTD data; pumps were simply positioned at estimated plume depth for these casts. No temperature or salinity anomalies could be discerned for any of the casts.

## 2.2. Sample Digestion and Analysis

Filters were subsampled using an acrylic template stainless steel scalpel, without rinsing of residual seasalt and while still frozen. Subsamples (14.8% of sample by filter area) were digested in closed 15mL Teflon screw-cap vials (Savillex) for 4 hours at ~100°C in a mixture of 1 mL concentrated HNO<sub>3</sub> (twice sub-boiling distilled in Teflon) and 50 μL HF (Ultrex, Baker), effecting a complete dissolution of the particulate and filter material. Digest solutions were diluted and analyzed for Al, Fe, Mn, and Ni using a Hitachi Z-9000 (Hitachi Instruments, Inc. Danbury CT) multielement graphite furnace atomic absorption spectrophotometer. Sample concentrations were determined by three point standard additions with an analytical

reproducibility better than 3%. REEs were determined by High Resolution Inductively Coupled Plasma Mass Spectrometry (HR-ICP-MS; ELEMENT, Finnigan MAT, Bremen, Germany) using a desolvating microconcentric nebulizer (MCN 6000, CETAC Corp., Omaha, NB). The REEs were determined to ±2% or better using a novel enriched isotope internal standardization scheme requiring no oxide interference corrections (Field and Sherrell, 1998). Importantly, this method provides inter-element ratios for the REEs which are significantly more precise than the individual elemental determinations; we estimate typical ratio precision better than 0.5%. We estimate that analytical and subsampling reproducibility contributed roughly equally to the overall precision of particulate metal concentrations in seawater, estimated at ~±5%.

Procedural blanks were determined on an unused filter and on the “dipped” blank; the latter was determined to be the more appropriate procedural blank and was subtracted from all sample concentrations. Because filters were not acid cleaned, blanks for some elements were significant. In particular, Ni blanks were up to 9% of sample concentration. Blank corrections for Al, Fe and Mn were <1.6% (largest corrections for background sample 3B) and for REEs were <1% for all samples.

## 3. RESULTS

Particulate Fe concentrations were expected to be highest near known high temperature vents, as has generally been found for other hydrothermal systems, but instead the opposite was found for our near-field samples. For these neutrally buoyant plume samples, particulate Fe concentrations varied from 10 nM at near-vent stations to 26 nM at distal stations, compared to 1.0 nM at background station 3B (Table 1). For most casts, samples from pumps T and B gave similar Fe concentrations (Table 1) indicating vertical particulate Fe homogeneity over the 14–21 m pump separation within each deployment. Thus, the 2.5-fold variation in particulate Fe is an inter-cast feature largely representing lateral variations in the plume. Surprisingly, the lowest Fe concentrations were found at cast locations closest to A and L Vents (Casts 6, 7, 10), and at similar distance from P vent, where transmission anomalies

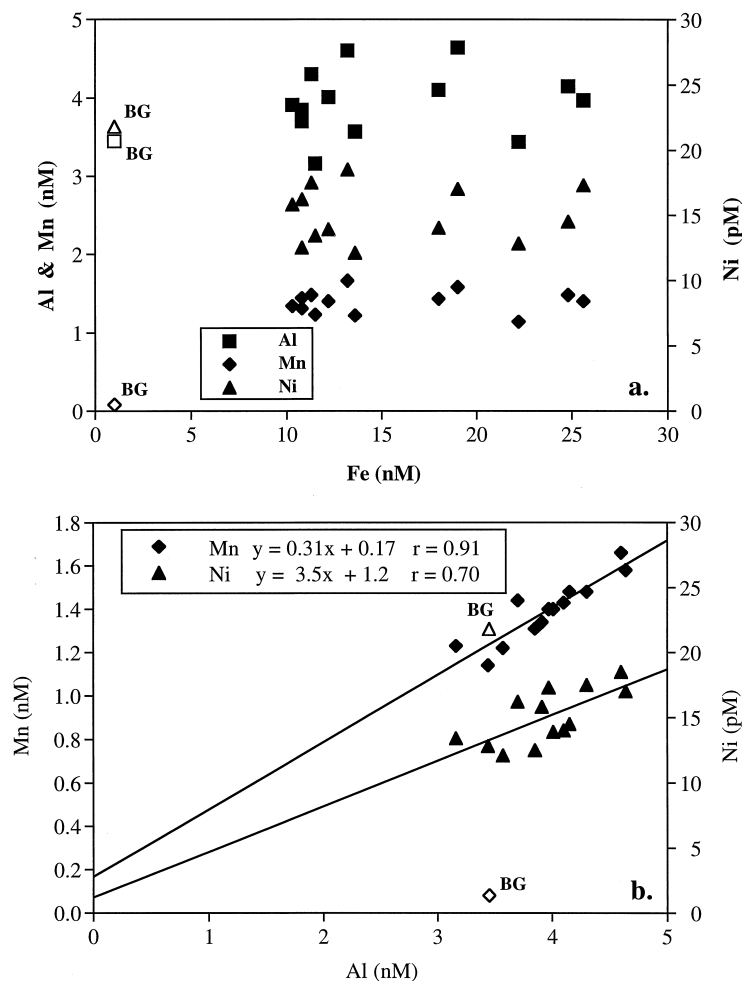


Fig. 2. (a) Particulate Al, Mn and Ni vs. Fe in for plume samples (closed symbols) and a background off-axis sample (open symbols marked BG). (b) Regression of Mn and Ni against Al in plume samples, with background Ni samples plotted for comparison.

were largest and narrowest. The highest Fe concentrations were found in Casts 11, 4 and 2 (bottom pump), which were located furthest from known high-temperature venting and were associated with attenuated and thicker, or negligible, transmission anomalies (Table 1, Fig. 1). The particulate Fe concentrations at 9°45'N are substantially lower than have been observed for near-field samples at TAG (German et al., 1991a; Trocine and Trefry, 1988), Juan de Fuca Ridge (JDFR: Feely et al., 1992), SEPR (Feely et al., 1996), and at 11°08'N along the EPR, just north of the Clipperton Transform Fault (Feely et al., 1994a).

Particulate manganese is elevated above background deep Pacific material by 8 to 16 times, whereas plume particulate Al (3.16 to 4.64 nM) is similar to or somewhat higher than background levels (3.45 nM), and Ni is lower in vent particulates (12.1–18.5 pM) than in background material (Sample 3B: 21.8 pM). All three of these elements vary over a relatively restricted range in plume samples, and show no relationship to particulate Fe or to distance from vent source (Table 1; Fig. 2a).

Concentrations of all 14 stable REEs are ~3–7 times enriched over background sample 3B (Table 1), and display smooth variations with atomic number (except Ce; see Fig. 3

and Discussion below). REE concentrations increase with particulate Fe, but REE/Fe ratios decrease with increasing Fe by a factor of 1.5–2.0 over the observed range of particulate Fe concentrations. In addition, the fractionation between light and heavy REEs becomes about 15% less LREE-enriched (expressed as Nd/Er ratio) with increasing Fe (see section 4.2, below).

#### 4. DISCUSSION

These REE data extend the available hydrothermal plume database into the Pacific. This provides an important constraint on REE behavior in plumes, because Pacific deepwater has a dissolved REE composition which is clearly distinct from that of Atlantic deepwater: the Pacific is enriched in concentration of all the REEs, but is also fractionated (LREE-depleted) relative to the Atlantic (Byrne and Sholkovitz, 1996; Piepgras and Jacobsen, 1992; Sholkovitz et al., 1994). Therefore, the 9°45'N plume data can be compared to published TAG data to evaluate whether the REE composition of plume particles reflects quantitatively the dissolved REE pool in ambient seawater.

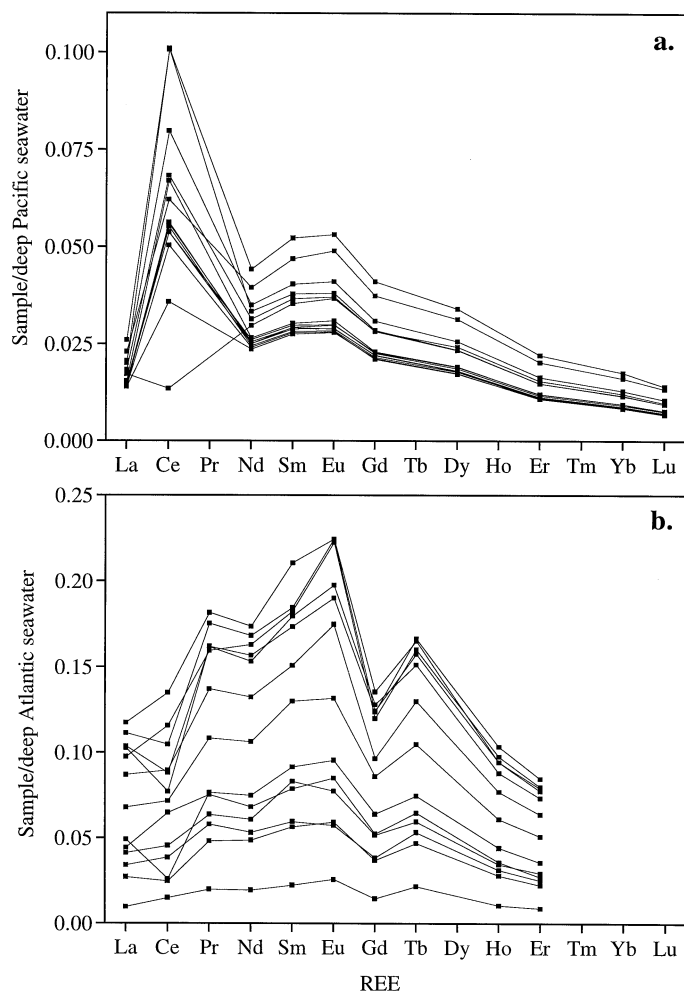


Fig. 3. Rare earth element (REE) patterns for background-corrected (by subtraction of the composition of off-axis background sample 3B, normalized to Al content of each plume sample), seawater normalized plume samples at (a) 9°45'N on the EPR and (b) TAG (German et al., 1990). Seawater concentrations for 9°45'N from Piepgras and Jacobsen (1992) and for TAG from German et al. (1990). Data points are missing for some elements, either because seawater data are not available (9°45'N) or because particles were analyzed only for a subset of REEs (TAG).

#### 4.1. Consistent Fractionation of REEs During Adsorption to Plume Particles in the Atlantic and Pacific

To compare REE fractionation patterns for hydrothermal particles in the Atlantic and Pacific plumes, we follow a practice commonly used in interpretation of trace metal trends in plumes, correcting for the contribution of non-hydrothermal particles by subtracting from particulate REE concentrations determined for nearby “background” samples. The assumption is that samples collected above the plume, or laterally displaced upstream of the plume (as for our samples) represent the composition of the ambient particle field into which the plume is mixed. While the presence of ridge-crest sediment resuspension may complicate this simple mixing picture, potentially diminishing the relevance of off-axis background samples, this simple approach is appropriate to a first-order comparison of REE uptake from seawater in an Atlantic vs. Pacific plume. The background-corrected hydrothermal abundances are then normalized to ambient dissolved REE concentrations to reveal the

fractionation patterns associated with uptake onto plume particles (Fig. 3).

The inter-element fractionation during uptake of REEs from seawater is apparently similar in the Atlantic and Pacific. The seawater-normalized REE patterns for the two plumes are both LREE-enriched (i.e., Nd/Er > 1.0; Fig. 3), with a superimposed “hump” in the middle REEs. The preferential MREE (Sm, Eu) uptake has been noted previously for suspended particles in the Sargasso Sea (Sholkovitz et al., 1994), hydrothermal sediments (German et al., 1993), ferromanganese crusts (De Carlo and McMurtry, 1992), and for oxide coatings on fossil foraminifera shells (Palmer and Elderfield, 1985); the MREE “hump” seems to be a ubiquitous aspect of REE fractionation during uptake from seawater onto authigenic oxides. The main differences in overall pattern shape results from anomalies for Ce and Gd which are unique to each data set. The Ce anomaly is generated by slow oxidation to insoluble Ce(IV) oxides, at a microbially mediated rate linked to that of Mn oxidation (Moffett, 1990).

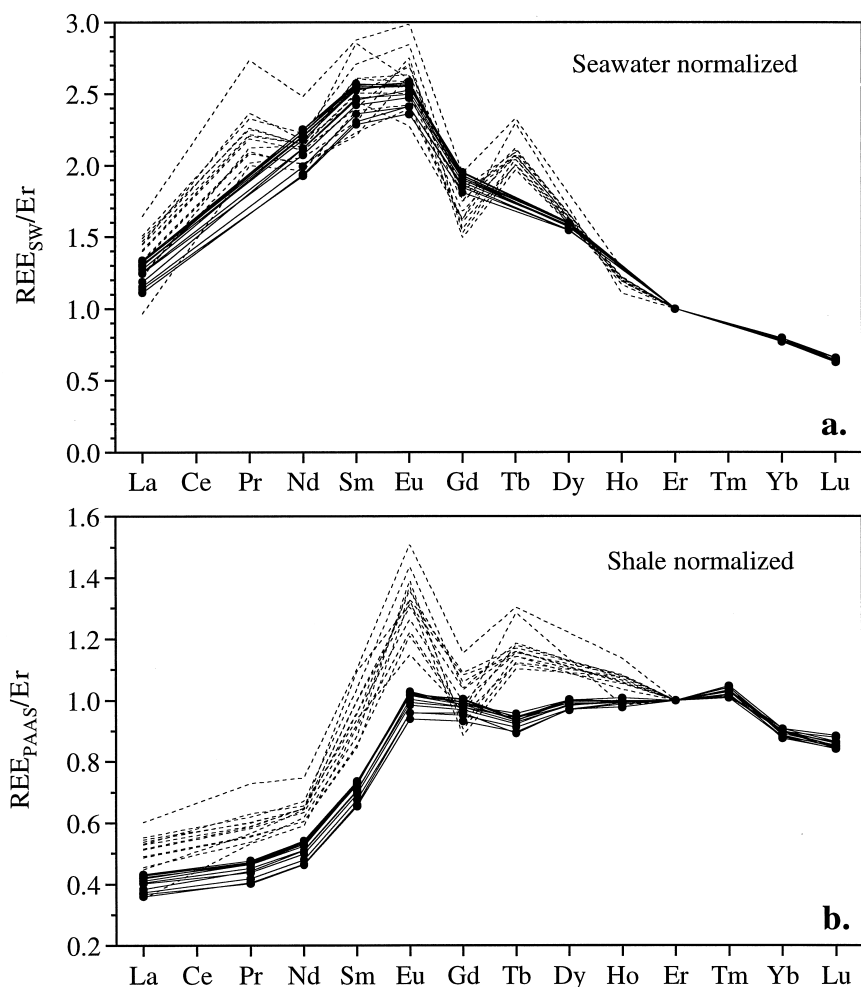


Fig. 4. REE in hydrothermal plume samples from TAG (no symbols, dashed line; German et al., 1990) and from 9°45' on the EPR (filled circles, solid lines), background-corrected using ratio of Al in plume sample to Al in non-plume background sample as indicator of background contribution to each sample, normalized to seawater or shale, then normalized to Er. (a) normalized to ambient dissolved REEs in Atlantic (German et al., 1990) and Pacific (Sta. 39-1, 2692m; Piepgras and Jacobsen, 1992), respectively. (b) normalized to Post-Archean Australian Shale (Taylor and McLennan, 1985). Data for Ce omitted for simplicity of presentation.

Thus, the Ce anomaly in Fig. 3 is related to the background-corrected Mn content of the plume particles. While the 9°45'N plume is enriched in Mn and shows substantial Ce anomalies, the TAG plume shows no particulate Mn enrichment relative to background, and there is little or no Ce anomaly for most samples (a few show small negative anomalies, suggesting some degree of over-correction for the true background). The other notable difference, a negative Gd anomaly at TAG, is probably an analytical artifact resulting from over-correction of the ICP-MS Gd signal for the contribution of LREE oxides, or undercorrection of the dissolved data used in the normalization (Field and Sherrell, 1998). For the purposes of the present discussion, we are interested in processes leading to the overall LREE/HREE fractionation in each plume, rather than the specific cause of the MREE "hump" or differences in Ce or Gd.

It is clear from Fig. 3 that there is a high degree of internal similarity for patterns within each plume. The vertical offsets of patterns within each plume and differences in absolute magnitude between the plumes simply reflect varying particulate Fe

concentrations. To compare quantitatively the mean fractionation patterns for each plume, we normalize all REEs to Er for each sample, and plot the REE patterns for each plume, normalized to both shale (as is conventional in the marine REE literature) and to ambient seawater (Fig. 4). Offsets between TAG and NEPR data for REEs other than Er then reveal even minor fractionation differences in a clear manner. This presentation of the data demonstrates that while each plume displays a small range in REE fractionation pattern, and these ranges are distinct when all data are normalized to shale, they become indistinguishable when normalized to appropriate local seawater (Fig. 4). The results indicate that REE fractionation associated with uptake from seawater is constant within the uncertainty represented by the small range of patterns observed in each plume. Differences in particulate Fe concentration, style of venting (Haymon et al., 1993; Humphris and Kleinrock, 1996; Rona and von Herzen, 1996), Fe/Mn ratio of plume particles, and dissolved speciation of the REEs (Byrne and Kim, 1993; Byrne and Sholkovitz, 1996) all seem to have

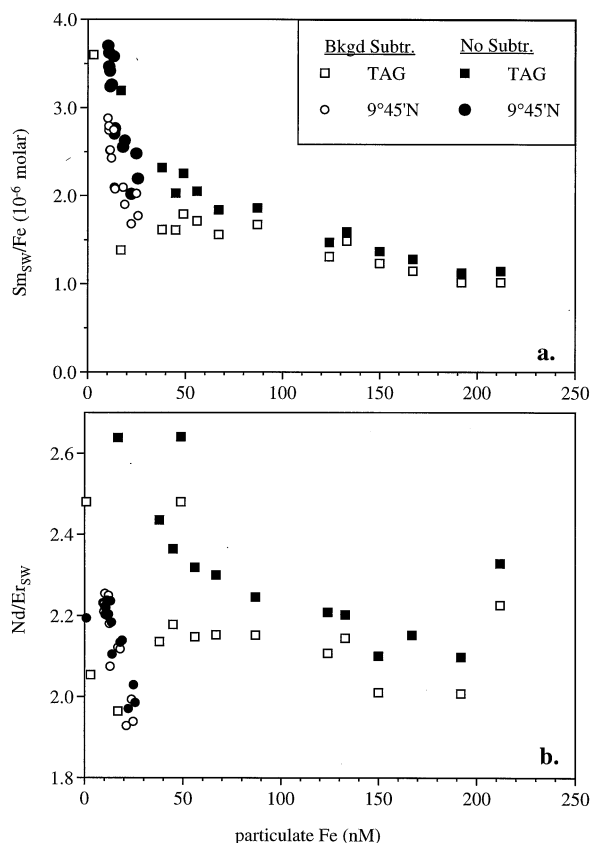


Fig. 5. Seawater normalized REE composition vs. Fe in particles from NEPR and TAG, with and without subtraction of composition of non-plume background sample. (a) Sm/Fe molar ratio; (b) Nd/Er molar ratio, an indicator of LREE/HREE fractionation.

minor effects on REE adsorption at this level of interpretation. However, we have not yet addressed the cause of the subtle but significant variations in REE patterns among samples within each plume.

#### 4.2. Within-Plume Variations in REE Composition With Particulate Fe Concentration

To investigate intra-plume differences in REE behavior it is necessary to evaluate REE with respect to Fe, the main component of freshly precipitated hydrothermal particles. We do this by considering REE/Fe (represented by Sm/Fe) and LREE/HREE fractionation (represented by Nd/Er) relative to particulate Fe concentration (Fig 5a,b). Both Sm/Fe and Nd/Er increase roughly linearly with decreasing Fe with the 9°45'N plume (Fig 5a,b). Subtraction of off-axis background particle composition (as above) alters the range and extent of the data in relatively subtle ways, decreasing and compressing somewhat the range of Sm/Fe ratios and expanding slightly the range of Nd/Er fractionation while leaving the mean Nd/Er unaffected (Fig. 5 a,b).

The comparable background-subtracted data from the TAG data set produces values for Sm/Fe and Nd/Er that are similar to those determined at 9°45'N, despite the fact that particulate Fe is much higher (Fig. 5a,b). The background subtraction

essentially eliminates the gradients in Sm/Fe and Nd/Er for TAG samples at <100 nM Fe. At higher Fe in the TAG plume, however, the decreasing trend in Sm/Fe with increased Fe persists. At TAG, the overall trend of increasing REE/Fe with decreasing Fe concentration has been interpreted to result from continued adsorption of REEs as the plume disperses and plume particles age (German et al., 1991a; German et al., 1990; Rudnicki and Elderfield, 1993). However, because particulate Fe increases with distance off-axis for the sampled segment of the 9°45'N plume (Fig. 1; Field and Sherrell, submitted), a consistent interpretation requires that older particles are found closer to the buoyant plume source and younger particles further from the source at 9°45'N. This inverse relationship between plume particle age and plume water age can be explained by slow Fe(II) oxidation and Fe(III) colloid coagulation to produce filterable (>0.45  $\mu\text{m}$ ) Fe particles at a fractional rate exceeding the fractional dilution rate, thereby producing an off-axis particulate Fe maximum within the neutrally buoyant plume (Field and Sherrell, submitted). These freshly precipitated primary hydrothermal precipitates are diluted into an existing background particle population which is ubiquitous in the near-bottom water column over the ridge axis, and contains much older (largely resuspended) hydrothermal particles. Similar slow oxidation and aggregation of colloids, occurring on the time scale of near-field plume advection, has been documented at Gorda Ridge (Massoth et al., 1999). The age-distance relationship at 9°45'N is supported by the finding that chalcophile element concentrations (Zn, Cd; Sherrell and Field, unpubl. data) decrease with distance off-axis (from Cast 6 to Cast 11; Fig. 1), consistent with rapid dissolution of sulfides precipitated in the buoyant plume (Feely et al., 1992; German et al., 1991a; Metz and Trefry, 1993). This explanation for the in-plume REE trends at 9°45'N clearly requires that the background particles have Sm/Fe values several times higher than that of recently precipitated hydrothermal Fe(III) particles and that the background signature is also more LREE-enriched (higher Nd/Er). We contend that the increasing Sm/Fe and Nd/Er with decreasing Fe at 9°45'N can be explained as a simple mixing between fresh Fe(III) precipitates and background material, rather than continued adsorption of REEs on the primary oxyhydroxide precipitates as they age on the time scale of plume advection over kilometers.

#### 4.3. A Mixing Model for REE Composition Variations in a Plume

An appropriate quantitative mixing model for the 9°45'N plume must not only explain the relatively modest but important REE composition variations (e.g., Nd/Er ratios vary by about 15%, about half the difference in Nd/Er between deep Pacific and deep Atlantic water; Byrne and Sholkovitz, 1996; Elderfield, 1988), it must also be able to reproduce the bulk composition of the plume particles, which vary in Fe-Al-Mn inter-element ratios. A mixing model can help to identify appropriate mixing endmembers and their REE composition. Our goal is a detailed evaluation of the range of fractionation patterns, to quantify fractionation associated with adsorption from seawater at a level of accuracy and precision similar to that of the REE determinations ( $\sim\pm 2\%$ ).

Particulate Al, Mn and Ni vary over a restricted range in our

9°45'N samples and are unrelated to particulate Fe (Fig. 2a). The apparent insensitivity of these particulate metals to Fe concentration and distance from source, combined with the Al and Mn enhancements relative to off-axis sample 3B, suggests that these elements trace the contribution of a background particle field which is unique to ridge-crest bottom water. Enrichment of particulate Al in the near-bottom water column is generally indicative of resuspended surface sediments, which have a higher fraction of terrigenous material relative to the composition of suspended matter in the water column (Dymond and Roth, 1988; Sherrell and Boyle, 1992; Sherrell et al., 1998; Feely et al., 1999). Although Al can also be adsorbed from seawater onto plume particles, estimated molar Al/Fe ratios resulting from this process are less than 0.01 (Elderfield et al., 1993); our observed Al/Fe is  $>0.15$ , far too large to result from adsorption. In addition, endmember vent fluid Al/Fe is generally  $<0.01$  (Von Damm, 1995), ruling out a hydrothermal source for the elevated particulate Al in the plume samples relative to background (3B). The relatively good correlation of Mn and Ni to Al (Fig. 2b), with small positive intercepts that are not statistically different from zero, suggests that these two elements are also dominated by a resuspended component. The high Mn content occurs because the residence time of particles in the surface sediments is apparently sufficient to allow microbial oxidation of dissolved Mn (Cowen et al., 1990; Lavelle et al., 1992), which does not occur to an appreciable degree over the time scale of plume advection to 2 km. Ridge-crest metalliferous sediments typically have Fe/Mn ratios of about 3.0–3.5 (Lyle, 1986), compared to 7–20 in our plume samples, and to  $\sim 60$  in high-Fe plume samples from the SEPR (Feely et al., 1996). Resuspension of ridge-crest sediments must therefore contribute Al and Mn, as well as some Fe component, to the Fe-rich primary plume.

Mixing of primary precipitates with ridge-crest background particles at 9°45'N is most easily visualized on an Al, Fe, and Mn mole fraction ternary diagram (Fig. 6). To determine mixing ratios for each sample, it is necessary to determine the composition of appropriate endmembers within the ternary plot. We assumed the primary hydrothermal precipitate endmember (HT) was equivalent to that of high-Fe samples from SEPR where intense plumes have suspended Fe concentrations of  $\geq 200$  nM, suggesting that particle types other than primary hydrothermal precipitates are negligible to overall composition (Feely et al., 1996). The HT endmember is 98% Fe (mole fraction of Fe+Al+Mn values from Table 2); the remaining 2% likely includes small contributions of Al and Mn(II) adsorbed to Fe oxyhydroxide surfaces. With the 9°45'N plume data, we plot on the same ternary diagram the larger data set of Feely et al. (1994a) for two segments of the NEPR (9°N and 11°N regions, separated by the Clipperton Transform Fault). Most of these samples lie along the same mixing line described by our samples, with the highest-Fe samples (from 11°10'N) approaching our HT endmember. The similarity of the two data sets indicates that interpretation within a single mixing model is valid. We assume that the lower-Fe samples of Feely et al. (1994a) missed the cores of plumes and sampled ridge-crest background material. The Fe-Al-Mn data of Feely et al. (1994a) allow an estimate of the composition of the second endmember representing the ridge-crest background particle field (on-axis BG). We plot this point on the extrapolation of

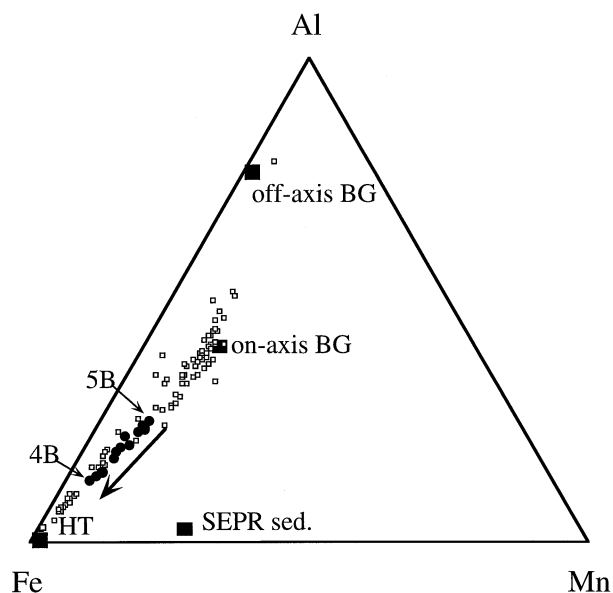


Fig. 6. Ternary diagram illustrating 2-endmember mixing model for Fe-Al-Mn composition of 9°45'N plume particles (closed circles). Large arrow indicates increasing distance from vent source. Endmembers are primary hydrothermal precipitates (HT) and ridge-crest background particles (on-axis BG). Sample 3B is plotted as "off-axis BG," and composition of hydrothermal metalliferous surface sediment on the southern EPR are marked "SEPR Sed." Note that on-axis BG endmember plots as a  $\sim 50:50$  mixture of off-axis BG particles, and the nearly pure metalliferous carbonate from the SEPR. Plume-depth samples from an along-axis survey of between 9° and 11°N (Feely et al., 1994) shown in open squares. See text for details.

the regression of our data to the highest Mn samples of Feely et al. (1994a), and list its composition in Table 2. The Fe-Al-Mn composition of the samples, and their fractions of each endmember, are listed in Table 3. It is clear that the new 9°45'N plume data fall in a range roughly midway between the two endmembers, while the more geographically extensive sampling of Feely et al. (1994a) for the whole ridge section south and north of the Clipperton Transform Fault covered a larger range of endmember mixtures. The off-axis background sample (3B) plots near the composition of crustal material, and is well off the mixing line described by the plume samples. A few samples from the earlier data set trend toward the off-axis background sample, suggesting secondary mixing of on- and off-axis background particle populations.

It is interesting to note that our ridge-crest background endmember plots as a  $\sim 50:50$  mixture of the off-axis background sample (3B) and the surface sediment composition from the SEPR (Marchig and Erzinger, 1986) (Fig. 6). We are aware of no measurements of the composition of surface sediments deposited on the NEPR, but it is reasonable to suggest that they represent a mixture of the almost pure hydrothermal carbonate found on the SEPR ridge-crest, and the proximal background water column particles, with substantial terrigenous (clay) component, represented by sample 3B. This would likely place the composition of 9°45'N surface sediment, which is resuspended to contribute to the apparently stable background endmember, somewhere along the mixing line between the SEPR sediment and the on-axis BG endmember (Fig. 6). Analyses of local

Table 2. Composition of mixing model endmembers, off-axis background particles and metalliferous sediments.

	Fe	Al (mole fraction)	Mn	Fe/Mn (molar)	Fe/Al (molar)	Sm <sub>SWR</sub> /Fe (10 <sup>-6</sup> molar)	Nd/Er <sub>SW</sub> (molar)
Endmembers							
Hydrothermal (HT)*	0.98	0.003	0.02	59.5	284.5	0.94	1.82
On-axis background (BG)	0.48	0.40	0.12	3.9	1.2	5.04	2.49
Other particle types:							
Off-axis background <sup>†</sup>	0.22	0.76	0.02	12.8	0.3	9.46	2.19
Metalliferous sediment <sup>#</sup>	0.74	0.04	0.23	3.3	18.7	3.73	2.70

\* Assumed equal to composition of high-Fe plume samples on the SEPR (Feely et al., 1996).

<sup>#</sup> Ridge-crest metalliferous sediments from the southern EPR (Marchig and Erzinger, 1986).

<sup>†</sup> Composition of off-axis suspended matter at 2100 m (sample 3B).

NEPR surface sediments, or very near-bottom suspended matter sampling, would help constrain the mixture of particle types which constitutes the on-axis background particle composition.

The mixing model results, combined with the measured REE compositional gradients, can be used to estimate the REE composition of the HT and on-axis BG endmembers. Regressions of Sm/Fe and Nd/Er against the fractional hydrothermal endmember contribution (% HT), determined from the Fe-Al-Mn mixing model, have very good correlation coefficients ( $r > 0.95$ ) and allow extrapolation to the REE composition of the HT (100% HT) and on-axis BG endmembers (0% HT). (Fig. 7 a,b). This analysis predicts that ridge-crest BG particles have Sm/Fe ratios about 5 fold higher than that of the pure hydrothermal precipitate endmember, and about 2 fold higher than mean plume particle composition. The seawater-normalized Nd/Er fractionation extrapolates to an enrichment of 1.82 for the primary precipitate endmember, increasing through the range of the plume samples to 2.49 in the BG particles. The mixing model suggests, then, that LREE are preferentially adsorbed from seawater onto hydrothermal particles (Nd/Er<sub>SW</sub>

> 1), but with somewhat less fractionation than is evident from the plume sample composition.

It is noteworthy that, despite the uptake of REE on these plume particles, Sm/Fe in all of the plume and background particles is about half or less of the Sm/Fe in off-axis particles which are presumed unaffected by hydrothermal activity (Fig. 7a). The shale component of the off-axis particles (calculated assuming total Al content represents a component with average shale composition) has somewhat lower Sm/Fe, suggesting that a significant fraction of REE reside in a low-Fe component of the background material which is less abundant in the on-axis background particles, probably an organic phase (Fig. 7a). The seawater normalized Nd/Er of off-axis background particles is, however, somewhat lower than that of the on-axis BG endmember, indicating less fractionation relative to seawater in the off-axis material. Average shale plots with very high Nd/Er, showing that LREE-enrichment during uptake from seawater does not compensate for the overall LREE-depletion of the ocean relative to shales (Fig. 7b).

The mixing model demonstrates that the most accurate comparison of fractionation in Pacific and Atlantic plumes would require that the composition of the appropriate HT endmember in each plume be known. This endmember represents unadulterated young hydrothermal precipitates whose REE composition should most directly reflect short-term uptake from seawater. In the 9°45' N plume, the pure HT component is difficult to sample because of the slow production of >0.45 μm Fe precipitates and the ubiquitous BG component. The time scale for increased REE adsorption (and Nd/Er fractionation), which is apparent in the on-axis BG composition, is uncertain; the inference of an important resuspension source suggests a potentially long residence time in surface sediment prior to a relatively short trip through the water column. We speculate that changes in REE composition of hydrothermal particles occur over time scales at least two orders of magnitude longer than particle residence time in the plume within a few km of the vent site.

The mixing model also speaks to the role of Mn in REE uptake. The trends in Sm/Fe and Nd/Er for the plume samples are well correlated with Fe/Mn because older resuspended BG particles are Mn-enriched while the HT endmember is almost Mn-free. It is important to note that this does not necessarily imply that Mn oxides in the sediments are responsible for the additional REE content and higher Nd/Er. We speculate that

Table 3. Sample composition and modeled endmember fractions.

Sample	Fe-Al-Mn composition			Endmember fractions	
	Fe	Al mole fraction	Mn (%)	HT (%)	on-axis BG (%)
3B*	22	76	2		
2B	82	14	5	68	32
2T	72	22	6	51	49
4B	83	13	4	72	28
4T	83	13	5	71	29
5B	66	25	9	35	65
5T	66	25	9	36	64
6B	68	24	9	38	62
6T	68	24	8	39	61
7B	68	23	9	37	63
7T	69	23	8	42	58
10B	74	19	7	52	48
10T	72	20	8	47	53
11B	75	18	6	55	45
11T	77	17	6	57	43

\* Off-axis background sample

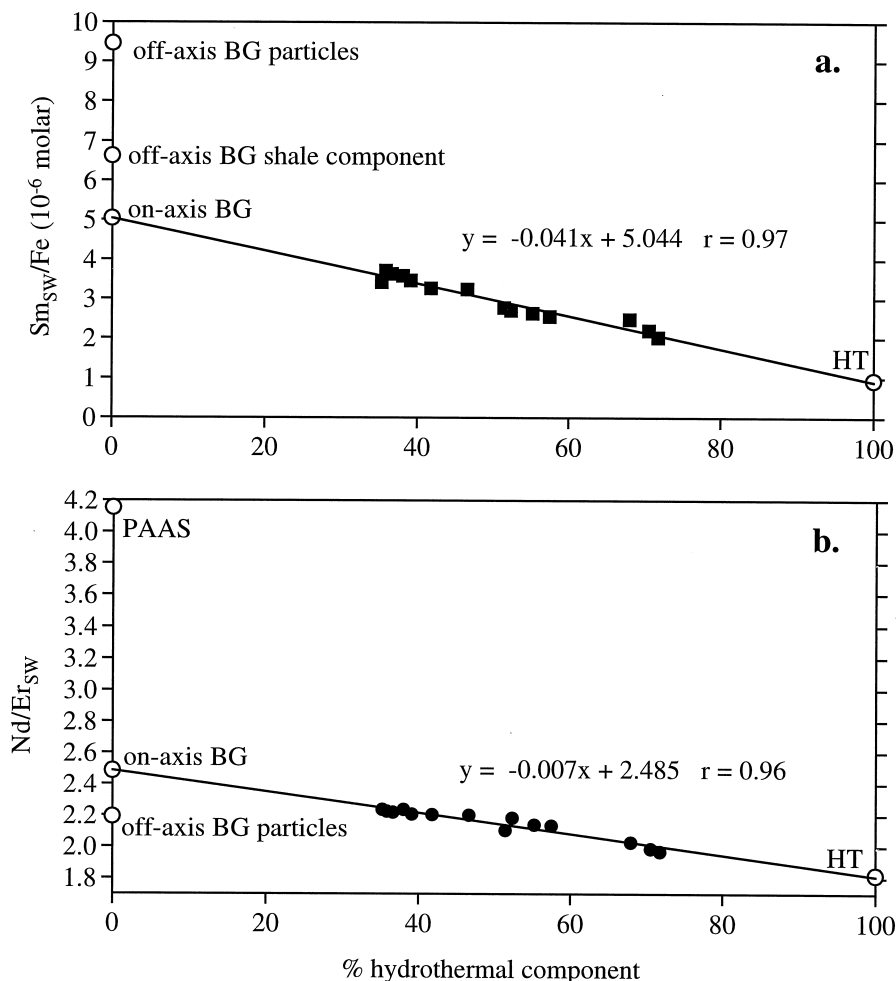


Fig. 7. Regressions of seawater normalized (a)  $Sm/Fe$  and (b)  $Nd/Er$  for  $9^{\circ}45'N$  plume samples against percent hydrothermal component derived from the mixing model (see text), demonstrating that REE composition is consistent with 2-endmember mixing between fresh hydrothermal precipitates (HT) and on-axis background (BG) particles. For comparison, measured  $Sm_{sw}/Fe$  for off-axis background particles and  $Sm_{sw}/Fe$  for shale (PAAS) component of off-axis background particles, assuming Al in background particles is shale-derived, are plotted in (a). To set LREE/HRRE fractionation in a larger geochemical context,  $Nd/Er_{sw}$  for shale (PAAS) and for off-axis background particles are plotted in (b) (see text for discussion).

aging of the Fe oxyhydroxides on the seafloor causes changes in the REE composition of these phases which are concomitant with Mn oxidation; Mn content may simply act as a tracer of the aging process. Such a Mn clock may be specific to NEPR sediments, and not apply to sediments near TAG. The seawater-normalized REE composition of the TAG plume (German et al., 1990; Figs. 4 and 5) may also be increased substantially by mixing with much older, possibly resuspended particles, despite the lack of Mn in these particles. There is some support for this hypothesis in a few more recent samples from the TAG plume (Ludford et al., 1996), which show REE/Fe values about half of those reported in German et al. (1990), perhaps reflecting a temporal decrease in contribution of older, high REE/Fe particle types. Background particulate Mn content along the ridge axis may reflect that of proximal surface sediments, which in turn may depend on sediment accumulation rate, microbially-catalyzed Mn oxida-

tion rate, or diffuse-flow Mn sources (Cowen et al., 1990). The overall similarity in REE composition of the NEPR and TAG plumes indicates that Mn oxides are not a significant host phase for REEs, in agreement with previous inferences based on the composition of ferromanganese crusts (De Carlo and McMurtry, 1992) and metalliferous sediments (Barrett and Jarvis, 1988).

#### 4.4. Depletion of the Dissolved REE Pool in High Particulate Fe Plumes

One potential problem with application of a similar mixing model to plume REE distribution in the TAG plume has not been addressed: mixing of particle populations with distinct chemical signatures cannot account for observed curvature in REE vs. Fe regressions at TAG (German et al., 1990; German et al., 1991a). Rather, the convex curvature of element vs. Fe regressions for REEs and other seawater scavenged elements

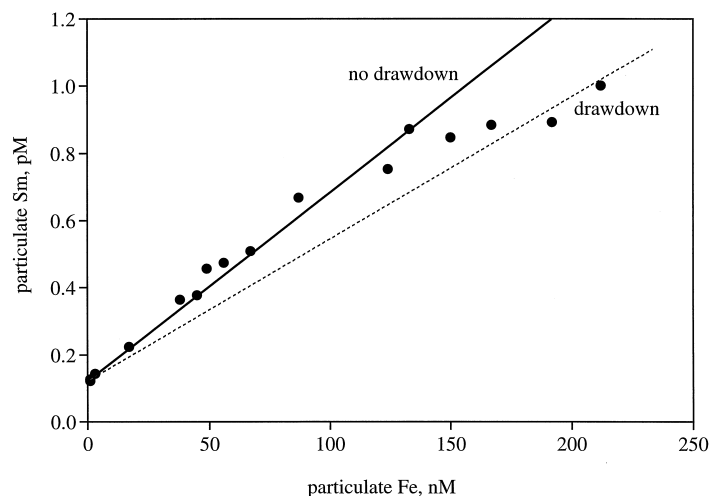


Fig. 8. Sm vs. Fe for TAG plume particles (after German et al., 1990), indicating response of particulate Sm to dissolved Sm drawdown at high particulate Fe (dashed line), and conservative mixing which would be observed in the case of no drawdown of the dissolved REE pool (solid line).

has been interpreted as resulting from continued uptake of these elements onto plume particles as they are diluted into ambient deepwater (German et al., 1990; German et al., 1991a; German et al., 1991b). We suggest that drawdown of the dissolved REE pool within high-particulate Fe plumes (Klinkhammer et al., 1983) may contribute to the observed curvature, resulting in decreased particulate REE/Fe at the high-Fe end of the mixing line, assuming constant  $K_d$  ( $= [g\ g^{-1}\ \text{particles}] \times [g\ g^{-1}\ \text{seawater}]^{-1}$ ). That is, at sufficiently high particulate Fe concentrations, the plume particles account for a substantial fraction of total REE in the water, while in ambient water the particulate fraction is only a few percent. Subsequent dilution of these high concentrations of Fe particles into ambient water, with  $K_d$  held constant, results in adjustment of the dissolved/particulate partitioning, pulling dissolved REE and REE/Fe in the particles back up to the conservative mixing line (Fig. 8).

This mechanism can be quantified as follows. The highest particulate Sm concentration (BG-corrected) in the TAG plume is equal to approximately 22% of the ambient deepwater dissolved Sm (0.90 vs. 4.13 pM; German et al., 1990). If ambient Sm is drawn down 22% in plume waters carrying  $\sim 200$  nM particulate Fe, the coexisting dissolved Sm would be  $\sim 3.23$  pM. Based on a suspended mass of  $\sim 40\ \mu\text{g}\ \text{kg}^{-1}$  at 200 nM particulate Fe (Trocine and Trefry, 1988), we estimate a  $K_d$  for Sm of  $7 \times 10^6$ . Applying this distribution coefficient to ambient particles for these deep Atlantic waters (background suspended mass of  $6\ \mu\text{g}\ \text{kg}^{-1}$ ; Sherrell, 1989), we predict a particulate Sm concentration in background samples of 0.17 pM or 4% of the dissolved Sm concentration. This Sm concentration only slightly overestimates that in low-Fe background samples near TAG (0.12–0.14 pM; German et al., 1990). With this constant  $K_d$  model, curvature results because continuous maintenance of adsorptive equilibrium results in increased particulate REE concentration (Sm/Fe) as the plume water is mixed back up to ambient deepwater REE concentrations. Curvature generated by a drawdown effect could be augmented by some degree of total REE loss through plume particle settling, or by settling loss of a low-REE, high-Fe sulfide phase

in the very proximal plume. These effects may dictate that curvature does not require continuous uptake within the young neutrally buoyant plume, *sensu* increasing  $K_d$  and disequilibrium with respect to REE adsorption, as suggested in previous work at TAG (German et al., 1990; German et al., 1991a). Further investigation of dissolved and particulate REEs in high-Fe plumes is required to test the drawdown vs. continuous uptake hypotheses. If the drawdown hypothesis is correct, then the lack of curvature observed for Sm vs. Fe in the  $9^{\circ}45'N$  plume (Table 1) is expected because particulate Fe does not reach high enough concentrations to cause significant depletion of the dissolved REE pool.

The potential for drawdown of the dissolved REE pool adds another complication to the determination of “canonical” values for REE uptake and fractionation onto hydrothermal oxyhydroxides. To avoid a confounding contribution from the background particles, it is most accurate to evaluate fractionation using plume samples from maximum particulate Fe portions of the plume. However, such plume regions are exactly where drawdown is expected; correction back to ambient (non-plume) dissolved concentrations using estimated  $K_d$  may be uncertain, and increasingly so with larger drawdown. Correction for expected drawdown in the TAG plume gives seawater-normalized Sm/Fe and Nd/Er values that are somewhat higher than the NEPR-derived HT endmember (Fig. 5a, b), suggesting that older particle types may be a fixture in this plume and in plumes at other vent sites. In practice, it may prove difficult to find a hydrothermal plume which has sufficiently high Fe and low background contribution to allow direct determination of the REE fractionation associated with initial uptake on pure hydrothermal precipitates, unless precise measurements of the sample filtrates are carried out as well.

The same argument for a drawdown effect holds for Y, Be,  $^{234}\text{Th}$  and  $^{210}\text{Pb}$  vs. Fe regressions at TAG (German et al., 1991a; German et al., 1991b), and suggests that the magnitude of curvature for these seawater-source elements and isotopes vs. Fe is driven by the degree of dissolved pool drawdown, which in turn is a function of (1) the reactivity of the element

with the initially precipitated Fe oxyhydroxides; and (2) the concentration of particulate Fe at the high-Fe end of the plume sample set. Because significant drawdown requires high particulate Fe concentrations, curvature of the regressions will vary with Fe dynamics in the plume. Gradients and absolute concentrations of particulate Fe are in turn a function of vent fluid Fe content, Fe removal through fallout of sulfides, Fe(II) oxidation kinetics, Fe(III) colloid aggregation kinetics and plume dilution rate (Field and Sherrell, submitted). Interpretation of such positive deviations from linear regression against Fe, for any element adsorbed from seawater onto hydrothermal plume particles, must accommodate this process and recognize that changes in particulate element/Fe ratios with dilution may occur without the continuous uptake resulting from an in-plume change in  $K_d$ .

### 5. CONCLUSIONS

1. The first measurements of particulate REE concentrations in a Pacific hydrothermal plume (9°45' on the EPR) allow comparison with published REE distributions in the TAG plume, Mid-Atlantic Ridge. REE fractionation varies over small ranges in each plume, but the mean background-corrected, seawater-normalized Nd/Er is indistinguishable in Pacific and Atlantic plumes.
2. Within the restricted range of REE composition measured within a few km of the vent source in the 9°45'N neutrally buoyant plume, Sm/Fe and Nd/Er increase linearly with decreasing particulate Fe.
3. Particulate composition variations within the 9°45'N plume can be explained by two-component mixing of primary hydrothermal precipitates with ambient ridge-crest background particles, which differ from the composition of off-axis, similar depth particles because of local resuspension input. A two-endmember mixing model accounts for both the variability in Fe-Al-Mn composition, and the changes in REE composition with particulate Fe in the 9°45'N plume. The calculated hydrothermal endmember is fractionated in Nd/Er by a factor of 1.8 relative to seawater.
4. Reinterpretation of published REE variations in the TAG plume suggests that curvature in the REE vs. Fe regressions may be caused by dissolved REE drawdown at high particulate Fe.
5. In general, particulate REE behavior in plumes is consistent with mixing of distinct particle populations of fixed composition, complicated in high particulate Fe plumes by local depletion of the dissolved REE pool. Previous explanations requiring kinetically slow continuous uptake of REE (changing  $K_d$ ) during dispersion of neutrally buoyant plume particles may be unnecessary, but cannot be ruled out in the absence of dissolved/particulate partitioning data for REEs in a high-Fe plume.
6. Elevated Sm/Fe and Nd/Er in the background resuspended endmember particles at 9°45'N suggests that further uptake and fractionation of REEs does occur, but probably only during residence on the sediment surface, on time scales much longer than the hours-days of near-field plume advection.
7. Based on the present results and REE data for TAG, Mn oxides do not appear to be an important carrier phase for adsorbed REEs.
8. If post-burial changes in the REE composition of hydrothermal metalliferous sediments are minimal, we speculate that a consistent relationship might be found between sediment REE patterns and those of the bottom water from which they were derived.

*Acknowledgments*—The authors acknowledge the able shipboard assistance of Laura Magde, Kathy Sullivan, and the Captain and crew of the R/V Atlantis II and the Alvin Group. We are grateful to Dan Fornari and Sandy Williams for the loan of the CTD and transmissometer. Harry Elderfield and Chris German provided insightful reviews of an earlier version which greatly improved this manuscript. This work was supported by NSF awards OCE 9217193 and OCE 9601668 to RMS and NSF award OCE 9504276 to GR.

### REFERENCES

- Barrett T. J. and Jarvis I. (1988) Rare-earth element geochemistry of metalliferous sediments from DSDP Leg 92: The East Pacific Rise transect. *Chem. Geol.* **67**, 243–259.
- Byrne R. H. and Kim K.-H. (1993) Rare earth precipitation and coprecipitation behavior: the limiting role of  $\text{PO}_4^{3-}$  on dissolved rare earth concentrations in seawater. *Geochim. Cosmochim. Acta* **57**, 519–526.
- Byrne R. H. and Sholkovitz E. R. (1996) The marine chemistry and geochemistry of the Lanthanides, in: *The Handbook of the Physics and Chemistry of Rare Earths*, (ed. A. Gschneider and L. Eyring), Vol. 23, pp. 497–593, Elsevier.
- Cowen J. P., Massoth G. J., and Feely R. A. (1990) Scavenging rates of dissolved manganese in a hydrothermal vent plume. *Deep-Sea Res.* **37**, 1619–1637.
- De Carlo E. H. and McMurtry G. M. (1992) Rare-earth element geochemistry of ferromanganese crusts from the Hawaiian Archipelago, central Pacific. *Chem. Geol.* **95**, 235–250.
- Dymond J. and Roth S. (1988) Plume dispersed hydrothermal particles: A time-series record of settling flux from the Endeavour Ridge using moored sensors. *Geochim. Cosmochim. Acta* **52**, 2525–2536.
- Elderfield H. (1988) The oceanic chemistry of the rare earth elements. *Phil. Trans. Royal Soc. London A* **325**, 105–126.
- Elderfield H., Greaves M. J., and Rudnicki D. (1993) Aluminum reactivity in hydrothermal plumes at the Mid-Atlantic Ridge. *J. Geophys. Res.* **98**, 9667–9070.
- Feely R. A., Baker E. T., Lebon G. T., Gendron J. F., Massoth G. J., and Mordy C. W. (1999) Chemical variations of hydrothermal particles in the 1996 Gorda Ridge Event and chronic plumes. *Deep-Sea Res. II* **45**, 2637–2664.
- Feely R. A., Baker E. T., Marumo K., Urabe T., Ishibashi J., Gendron J., Lebon G. T., and Okamura K. (1996) Hydrothermal plume particles and dissolved phosphate over the superfast-spreading southern East Pacific Rise. *Geochim. Cosmochim. Acta* **60**, 2297–2323.
- Feely R. A., Geiselman T. L., Baker E. T., Massoth G. J., and Hammond S. R. (1990) Distribution and composition of buoyant and non-buoyant hydrothermal plume particles from the ASHES vent at Axial Volcano, Juan de Fuca Ridge. *J. Geophys. Res.* **95**, 12855–12874.
- Feely R. A., Gendron J. F., Baker E. T., and Lebon G. T. (1994a) Hydrothermal plumes along the East Pacific Rise, 8°40' to 11°50'N: Particle distribution and composition. *Earth Planet. Sci. Lett.* **128**, 19–36.
- Feely R. A., Massoth G. J., Baker E. T., Lebon G. T., and Geiselman T. L. (1992) Tracking the dispersal of hydrothermal plumes from the Juan de Fuca Ridge using suspended matter compositions. *J. Geophys. Res.* **97**, 3457–3468.
- Feely R. A., Massoth G. J., Trefry J. H., Baker E. T., Paulson A. J., and Lebon G. T. (1994b) Composition and sedimentation of hydrothermal plume particles from North Cleft segment, Juan de Fuca Ridge. *J. Geophys. Res.* **99**, 4985–5006.
- Field M. P. and Sherrell R. M. (1998) Magnetic sector ICPMS with desolvating micronebulization: Interference-free subpicogram deter-

- mination of rare earth elements in natural samples. *Anal. Chem.* **70**, 4480–4486.
- German C. R., Bourles D. L., Brown E. T., Hergt J., Colley S., Higgs N. C., Ludford E. M., Nelsen T. A., Feely R. A., Raisbeck G., and You F. (1997) Hydrothermal scavenging on the Juan de Fuca Ridge:  $^{230}\text{Th}_{\text{ss}}$ ,  $^{10}\text{Be}$ , and REEs in ridge-flank sediments. *Geochim. Cosmochim. Acta* **61**, 4067–4078.
- German C. R., Campbell A. C., and Edmond J. M. (1991a) Hydrothermal scavenging at the Mid-Atlantic Ridge: Modification of trace element dissolved fluxes. *Earth Planet. Sci. Lett.* **107**, 101–114.
- German C. R., Fleer A. P., Bacon M. P., and Edmond J. M. (1991b) Hydrothermal scavenging at the Mid-Atlantic Ridge: Radionuclide distributions. *Earth Planet. Sci. Lett.* **105**, 170–181.
- German C. R., Higgs N. C., Thomson J., Mills R., and Elderfield H. (1993) A geochemical study of metalliferous sediment from the TAG hydrothermal mound, 26°08'N, Mid-Atlantic Ridge. *J. Geophys. Res.* **98**, 9683–9692.
- German C. R., Klinkhammer G. P., Edmond J. M., Mitra A., and Elderfield H. (1990) Hydrothermal scavenging of rare-earth elements in the ocean. *Nature* **345**(6275), 516–518.
- Haymon R. M., Fornari D. J., Damm K. L. V., Lilley M. D., Perfit M. R., Edmond J. M., W. C. Shanks I., Lutz R. A., Grebeier J. M., Carbotte S., Wright D., McLaughlin E., Smith M., Beedle N., and Olson E. (1993) Volcanic eruption of the mid-ocean ridge along the East Pacific Rise at 9°45'–52'N: Direct submersible observations of seafloor phenomena associated with an eruption event in April, 1991. *Earth Planet. Sci. Lett.* **119**, 85–101.
- Humphris S. E. and Kleinrock M. C. (1996) Detailed morphology of the TAG active hydrothermal mound: Insights into its formation and growth. *Geophys. Res. Lett.* **23**, 3443–3446.
- Humphris S. E., Zirenberg R. A., Mullineaux L. S., and Thomson R. E. (1995) *Seafloor Hydrothermal Systems: Physical, Chemical, Biological, and Geological Interactions*. American Geophysical Union.
- Kadko D., Baker E., Alt J., and Baross J. (1994a) Global impact of submarine hydrothermal processes. RIDGE/VENTS Workshop.
- Kadko D., Baross J. and Alt J. (1995) The magnitude and global implications of hydrothermal flux. In *Seafloor Hydrothermal Systems* (ed. D.E. Humphris et al.) pp. 446–466. American Geophysical Union.
- Kadko D., Feely R., and Massoth G. (1994b) Scavenging of  $^{234}\text{Th}$  and phosphorus removal from the hydrothermal effluent plume over the North Cleft segment of the Juan de Fuca Ridge. *J. Geophys. Res.* **99**, 5017–5024.
- Klinkhammer G., Elderfield H., and Hudson A. (1983) Rare earth elements in seawater near hydrothermal vents. *Nature* **305**, 185–188.
- Lavelle J. W., Cowen J. P., and Massoth G. J. (1992) A model for the deposition of hydrothermal manganese near ridge crests. *J. Geophys. Res.* **97**, 7413–7427.
- Ludford E. M., Palmer M. R., German C. R., and Klinkhammer G. P. (1996) The geochemistry of Atlantic hydrothermal particles. *Geophys. Res. Lett.* **23**, 3503–3506.
- Lupton J. E., Baker E. T., Mottl M. J., Sansone F. J., Wheat C. G., Resing J. A., Massoth G. J., Measures C. I., and Feely R. A. (1993) Chemical and physical diversity of hydrothermal plumes along the East Pacific Rise, 8°45'N to 11°50'N. *Geophys. Res. Lett.* **20**, 2913–2916.
- Lyle M. W. (1986) Major element composition of Leg 92 sediments. In *Initial Reports of the Deep Sea Drilling Project* (ed. D. K. R. e. a. M. Leinen), Vol. 92, pp. 355–370. U.S. Gov. Print. Off.
- Marchig V. and Erzinger J. (1986) Chemical composition of Pacific sediments near 20°S: Changes with increasing distance from the East Pacific Rise. In *Initial Reports of the Deep Sea Drilling Project Leg 92* (ed. D. K. R. e. a. M. Leinen), Vol. 92, pp. 371–381. U.S. Gov. Print. Off.
- Massoth G. J., Baker E. T., Feely R. A., Lupton J. E., Collier R. W., Gendron J. F., Roe K. K., Maenner S. M., and Resing J. A. (1999) Manganese and iron in hydrothermal plumes resulting from the 1996 Gorda Ridge Event. *Deep-Sea Res. II* **45**, 2683–2712.
- Massoth G. J., Baker E. T., Lupton J. E., Feely R. A., Butterfield D. A., Damm K. L. V., and Roe K. K. (1994) Temporal and spatial variability of hydrothermal manganese and iron at cleft segment, Juan de Fuca Ridge. *J. Geophys. Res.* **99**, 4905–4923.
- Metz S. and Trefry J. H. (1993) Field and laboratory studies of metal uptake and release by hydrothermal precipitates. *Journal of Geophysical Research* **98**, 9661–9666.
- Michard A. (1989) Rare earth element systematics in hydrothermal fluids. *Geochim. Cosmochim. Acta* **53**, 745–750.
- Moffett J. W. (1990) Microbially mediated cerium oxidation in sea water. *Nature* **345**, 421–423.
- Mottl M. J. and McConachy T. F. (1990) Chemical processes in buoyant hydrothermal plumes on the East Pacific Rise near 21 N. *Geochim. Cosmochim. Acta* **54**, 1911–1927.
- Mottl M. J., Sansone F. J., Wheat C. G., Resing J. A., Baker E. T., and Lupton J. E. (1995) Manganese and methane in hydrothermal plumes along the East Pacific Rise, 8°40' to 11°50'N. *Geochim. Cosmochim. Acta* **59**, 4147–4165.
- Olivarez A. M. and Owen R. M. (1989) REE/Fe variations in hydrothermal sediments: Implications for the REE content of seawater. *Geochim. Cosmochim. Acta* **53**, 757–762.
- Palmer M. R. and Elderfield H. E. (1985) Rare earth elements in foraminifera tests. *Earth Planet. Sci. Lett.* **73**, 285–298.
- Pieprgas D. J. and Jacobsen S. B. (1992) The behavior of rare earth elements in seawater: Precise determination of variations in the North Pacific water column. *Geochim. Cosmochim. Acta* **56**, 1851–1862.
- Reid J. L. (1982) Evidence of an effect of heat flux from the East Pacific Rise upon the characteristics of the mid-depth waters. *Geophys. Res. Lett.* **9**, 381–384.
- Rona P. A. and von Herzen R. P. (1996) Introduction to special section on measurements and monitoring at the TAG hydrothermal field, Mid-Atlantic Ridge 26°N, 45°W. *Geophys. Res. Lett.* **23**, 3427–3430.
- Rudnicki M. D. and Elderfield H. (1993) A chemical model of the buoyant and neutrally buoyant plume above the TAG vent field, 26 degrees N, Mid-Atlantic Ridge. *Geochim. Cosmochim. Acta* **57**, 2939–2957.
- Ruhlin D. E. and Owen R. M. (1986) The rare earth element geochemistry of hydrothermal sediments from the East Pacific Rise: Examination of a seawater scavenging mechanism. *Geochim. Cosmochim. Acta* **50**, 393–400.
- Sherrell R. M. (1989) The trace metal geochemistry of suspended oceanic particulate matter. Ph.D dissertation, MIT/WHOI.
- Sherrell R. M. (1991) Collection of oceanic SPM for trace metal analysis using a new in situ pump. In *Marine Particles: Analysis and Characterization*, *Geophys. Monograph Ser.* (ed. D. C. Hurd and D. W. Spencer), Vol. 63, pp. 285–294. AGU.
- Sherrell R. M. and Boyle E. A. (1992) The trace metal composition of suspended particles in the oceanic water column near Bermuda. *Earth Planet. Sci. Lett.* **111**, 155–174.
- Sherrell R. M., Field M. P., and Gao Y. (1998) Temporal variability of suspended mass and composition in the northeast Pacific water column: Relationships to sinking flux and lateral advection. *Deep-Sea Res. II* **45**, 733–761.
- Sholkovitz E. R., Landing W. M., and Lewis B. L. (1994) Ocean particle chemistry: The fractionation of rare earth elements between suspended particles and seawater. *Geochim. Cosmochim. Acta* **58**(7), 1567–1579.
- Taylor S. R. and McLennan S. M. (1985) *The Continental Crust: Its Composition and Evolution*. Blackwell.
- Trocine R. P. and Trefry J. H. (1988) Distribution and chemistry of suspended particles from an active hydrothermal vent site on the Mid-Atlantic Ridge at 26 N. *Earth Planet. Sci. Lett.* **88**, 1–15.
- Von Damm K. L. (1995) Controls on the chemistry of temporal variability of seafloor hydrothermal fluids. In *Seafloor Hydrothermal Systems* (ed. S. E. Humphris et al.), pp. 222–247. American Geophysical Union.
- Von Damm K. L., Oosting S. E., Kozlowski R., Buttermore L. G., Colodner D. C., Edmonds H. N., Edmond J. M., and Grebmeier J. M. (1995) Evolution of East Pacific Rise hydrothermal vent fluids following a volcanic eruption. *Nature* **375**, 47–50.